Journal of Molecular Catalysis A: Chemical 424 (2016) 393–401

Contents lists available at ScienceDirect

Journal of Molecular Catalysis A: Chemical

journal homepage: www.elsevier.com/locate/molcata

Fullerol modification ferrihydrite for the degradation of acid red 18 under simulated sunlight irradiation

Tianyuan Xu[a,b], Runliang Zhu[a,*], Jing Liu[a,b], Qing Zhou[a], Jianxi Zhu[a], Xiaoliang Liang[a], Yunfei Xi[c], Hongping He[a]

[a] CAS Key Laboratory of Mineralogy and Metallogeny/Guangdong Provincial Key Laboratory of Mineral Physics and Material Research & Development, Guangzhou Institute of Geochemistry, Chinese Academy of Sciences, 511 Kehua Street, Guangzhou 510640, China
[b] University of Chinese Academy of Sciences, 19 Yuquan Road, Beijing 100049, China
[c] Nanotechnology and Molecular Science Discipline, Faculty of Science and Engineering, Queensland University of Technology, 2 George Street, GPO Box 2434, Brisbane, QLD 4000, Australia

ARTICLE INFO

Article history:
Received 8 July 2016
Received in revised form
14 September 2016
Accepted 15 September 2016
Available online 17 September 2016

Keywords:
Fullerol
Ferrihydrite
Simulated sunlight
Heterogeneous photo-Fenton

ABSTRACT

Fullerol (polyhydroxyfullerene, PHF) has shown favorable electron accepting properties in semiconductor photocatalytic systems, but little is known about the possibility of electron transfer mediation of PHF in heterogeneous photo-Fenton processes. This work intends to investigate the effect of PHF on the heterogeneous photo-Fenton activity of ferrihydrite (Fh). PHF/ferrihydrite (PHF/Fh) composites were prepared and their photo-Fenton activities in the degradation of acid red 18 under simulated sunlight irradiation were examined. The structural characteristics of the as-synthesized samples were studied using XRD, SEM-EDS, SPM, DRS, and N_2 adsorption-desorption. The results showed that PHF/Fh had much higher catalytic activities than Fh, and appropriate contents of PHF on PHF/Fh could enhance the stability of Fh. In addition, the presence of PHF on PHF/Fh could enhance the production of $^1O_2$ and •OH as compared with pure Fh. We propose that the excited state PHF could efficiently sensitize the ground state O_2 to generate $^1O_2$, and at the same time could transfer electrons to the Fe^{3+} on Fh, leading to an accelerated reduction of Fe^{3+} to Fe^{2+}. As a result, the decomposition of H_2O_2 (by Fe^{2+}) into •OH could be promoted as well. On the other hand, based on the results of GAMESS calculation and GC–MS analysis, the degradation pathway of AR18 was further proposed.

1. Introduction

Fullerene (C_{60}) possesses unique electronic properties and has potential applications in a variety of areas, *e.g.*, as photovoltaic and photocatalytic materials [1–3]. The excited state C_{60} and its derivatives such as fullerol (polyhydroxyfullerene, PHF) are able to generate $^1O_2$, a selective oxidant useful in applications such as photocatalysis for wastewater treatment, through photosensitization [4–7]. On the other hand, C_{60} and PHF in the electron-transfer processes can efficiently arouse a rapid photoinduced charge separation and a relatively slow charge recombination [8]; and thus they have been frequently studied as electron acceptors or electron carriers for enhancing charge separation in many semiconductor photocatalytic systems, such as PHF/TiO_2 [9,10], CdS-C_{60}/TiO_2 [11], C_{60}/ZnO [12], and C_{60}/Bi_2WO_6 [13]. On the other hand, heterogeneous photo-Fenton process, as another type of advanced oxidation technique, has also drawn extensive concerns in wastewater treatment, and this process also relies on the transition of electrons to Fe^{3+} (for the purpose of producing Fe^{2+}). However, to the best of our knowledge, little is known about the capability of electron transfer mediation by C_{60}/PHF in a heterogeneous photo-Fenton process.

As we know, the effectiveness of heterogeneous photo-Fenton reaction relies on the photolysis of Fe^{3+} in acidic media to yield Fe^{2+}, in conjunction with the reaction between Fe^{2+} and H_2O_2 to produce •OH [14,15]. In addition, the reduction of Fe^{3+} to Fe^{2+} could be accelerated by the photo-induced electrons from the adsorbed photochemical organic substrates such as the adsorbed dyes [16,17]. Moreover, recent studies also showed that the introduction of semiconductor materials (*e.g.*,TiO_2, $BiVO_4$) can accelerate the reduction of Fe^{3+} to Fe^{2+} by providing photo-induced electrons from semicon-

* Corresponding author.
E-mail address: zhurl@gig.ac.cn (R. Zhu).

http://dx.doi.org/10.1016/j.molcata.2016.09.024
1381-1169/

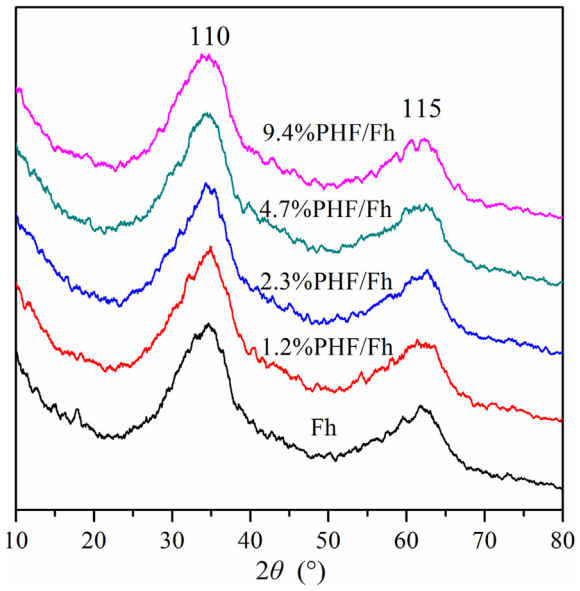

Fig. 1. The XRD patterns of Fh and PHF/Fh.

ductors [18,19]. Enlightened by these studies, we expect that the presence of PHF on heterogeneous photo-Fenton catalysts might transfer electrons from excited state PHF to Fe^{3+} under sunlight irradiation, which would then accelerate the reduction of Fe^{3+} to Fe^{2+} and thus improve the photo-Fenton catalytic activity for the degradation of organic compounds.

A variety of iron-based materials have been developed as heterogeneous photo-Fenton catalysts [20–22]. Among them, ferrihydrite (Fh) has drawn much attention as it is a naturally occurring Fe(III) hydroxide nanomineral with large specific surface area (SSA > 200 m^2/g) and abundant chemical active surface groups [23–27]. Wang et al. reported that Fh had good photo-Fenton catalytic performance for the oxidative decomposition of Mordant Yellow 10 under UV irradiation [28]. Fh may have strong interaction with PHF, as PHF generally presents negatively charged surface in the pH range 3.0–9.5 while Fh shows positively charged surface at pH < 8 [29,30]. Moreover, they may form surface composites through the formation of covalent bonds between the surface hydroxyl group on Fh and PHF. Theoretically, the excited state PHF could inject electrons to Fe^{3+} under sunlight irradiation due to $E^0(C_{60}^+/{}^1C_{60}^*) = 0.1$ V *vs.* NHE < $E^0(Fe^{3+}/Fe^{2+}) = 0.77$ V *vs.* NHE [9,31]. Thus, the combination of Fh and PHF might be an ideal approach to achieve enhanced electron transition mediation for the purpose of enhancing the photo-Fenton catalytic activity by accelerating electron transfer from PHF to Fh (*i.e.*, improving the reduction rate of Fe^{3+} to Fe^{2+}). This study aimed to investigate the effect of PHF on the heterogeneous photo-Fenton reactivity of Fh. PHF/Fh composites with different PHF contents were first synthesized. The microstructure of the resulting materials and their photo-Fenton catalytic activities in the degradation of acid red 18 (AR18) were studied, and the degradation mechanism of AR18 was further investigated. The results of this work showed that PHF could effectively improve the photo-Fenton activity of Fh for the degradation of AR18.

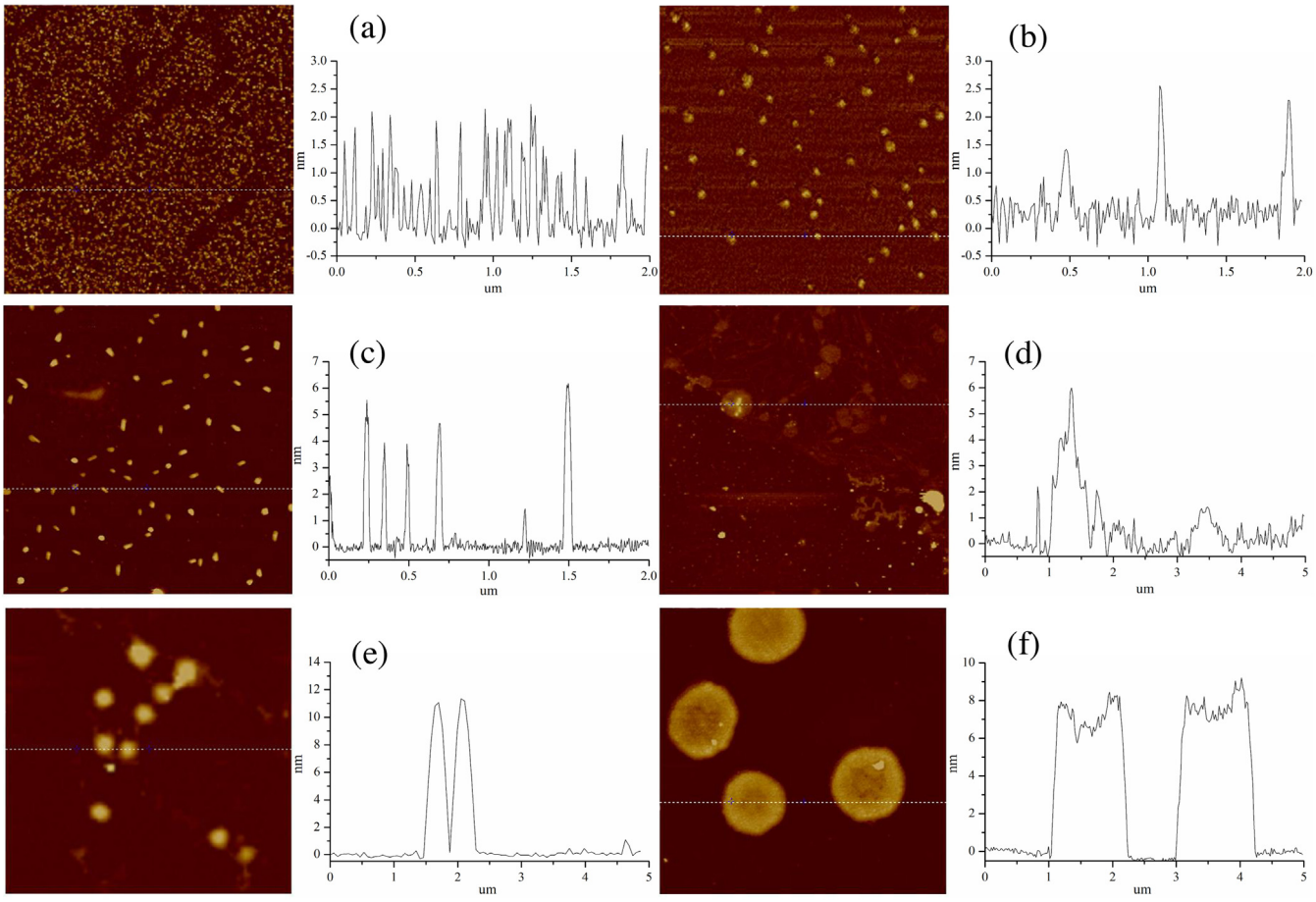

Fig. 2. SPM particle size analysis of PHF (a), Fh (b), 1.2%PHF/Fh (c), 2.3% PHF/Fh (d), 4.7%PHF/Fh (e), and 9.4%PHF/Fh (f).

Table 1
The carbon element contents and SSA results of various samples.

samples	C (wt%)	SSA (m^2/g)
Fh	–	263.6
1.2%PHF/Fh	0.81	255.2
2.3%PHF/Fh	1.26	241.7
4.7%PHF/Fh	2.06	228.8
9.4%PHF/Fh	3.67	203.3

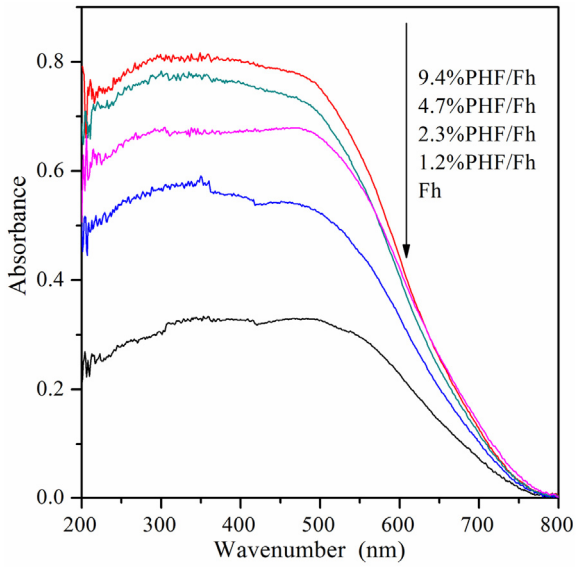

Fig. 3. UV–vis diffuse reflectance spectra of samples.

2. Experimental sections

2.1. Materials

High-purity (99%) PHF ($C_{60}(OH)_{21}\cdot 6H_2O$) was purchased from Suzhou Dade Carbon Nanotechnology CO., Ltd, China. AR18 was purchased from National Medicine Group Chemical Reagent Co., Ltd., China (Fig. S1). Other chemicals were obtained from the Guangzhou Chemical Reagent Factory, China. All the chemicals were of analytical grade and were used without further purification.

2.2. Preparation of catalysts

Fh was prepared by slowly and simultaneously titrating $Fe(NO_3)_3$ (1 M, 40 mL) and NaOH (6 M, 20 mL) into 10 mL ultrapure water, with vigorous magnetic stirring and controlling the solution pH at 7 ± 0.2. After continuous magnetic stirring for another 30 min, the products were centrifuged and washed.

The PHF/Fh was prepared by slowly and simultaneously titrating $Fe(NO_3)_3$ (1 M, 40 mL) and NaOH (6 M, 20 mL) into a solution (50, 100, 200, or 400 mL) containing 1 g/L PHF, with vigorous stirring and controlling the solution pH at 7 ± 0.2. After continuous magnetic stirring for another 30 min, the products were centrifuged and washed. According to the PHF content, the resulting materials were denoted as 1.2%PHF/Fh, 2.3%PHF/Fh, 4.7%PHF/Fh, and 9.4%PHF/Fh, respectively.

The PHF solutions were sonicated for 30 min before use. All of the obtained samples were freeze-dried under −40 °C, and pulverized to pass through a 200-mesh sieve.

2.3. Characterization

X-ray diffraction (XRD) patterns of the prepared samples were recorded by a Bruker D8 ADVANCE X-ray diffractometer. The measurements were operated at 40 kV and 40 mA with Cu Kα irradiation, and the 2θ range between 10° and 80° was recorded with a scanning speed of 2°/min. The carbon element contents were recorded by a Vario EL cube elemental analyzer (Elementar, Germany).

Scanning electron microscopy (SEM, Carl Zeiss SUPRA55SAPPHIR) was used to observe the surface state and structure of the photocatalysts. Scanning probe microscopy (SPM) characterization was performed on a Bruker Multimode controlled by a Nanoscope V controller. The particle size of the samples was measured from the protrusion height observed on a mica plate. A highly diluted aqueous suspension of samples was dropped on a mica plate and then dried for SPM characterization.

The UV–vis diffuse reflectance spectra (DRS) were obtained on Shimadzu UV-2550 double-beam digital spectrophotometer, and $BaSO_4$ was used as reference. Nitrogen adsorption-desorption isotherms were measured on a Micromeritics ASAP 2020 M instrument. Before the adsorption tests, the samples were degassed for 48 h at 30 °C. The multiple-point Brunauer-Emmett-Teller (BET) method was used to calculate the SSA of the samples.

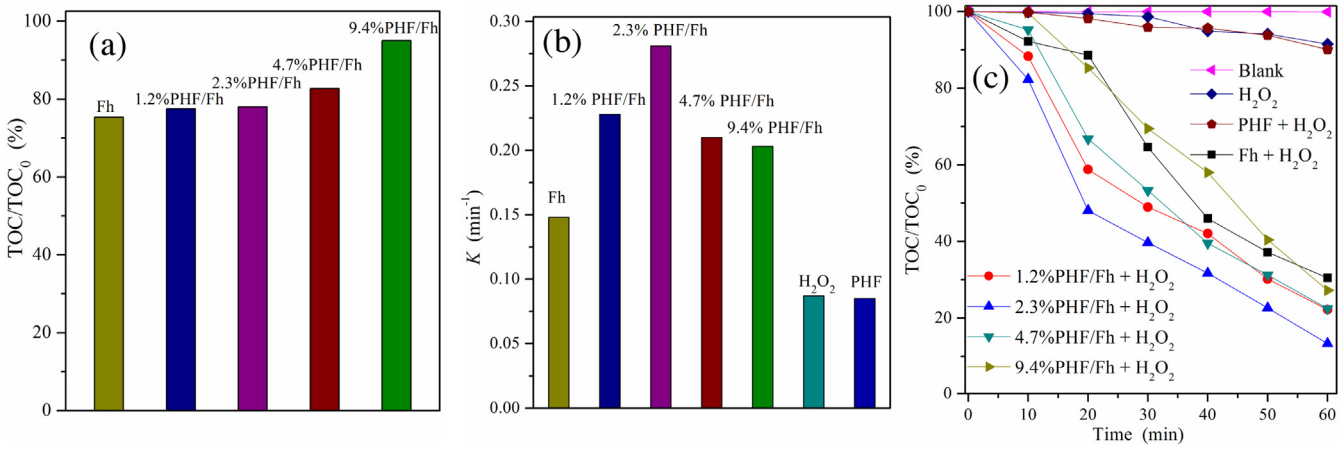

Fig. 4. The adsorption of acid red 18 in dark (a), decolorization kinetics (b) and mineralization (c) of acid red 18 with H_2O_2 under sunlight irradiation.

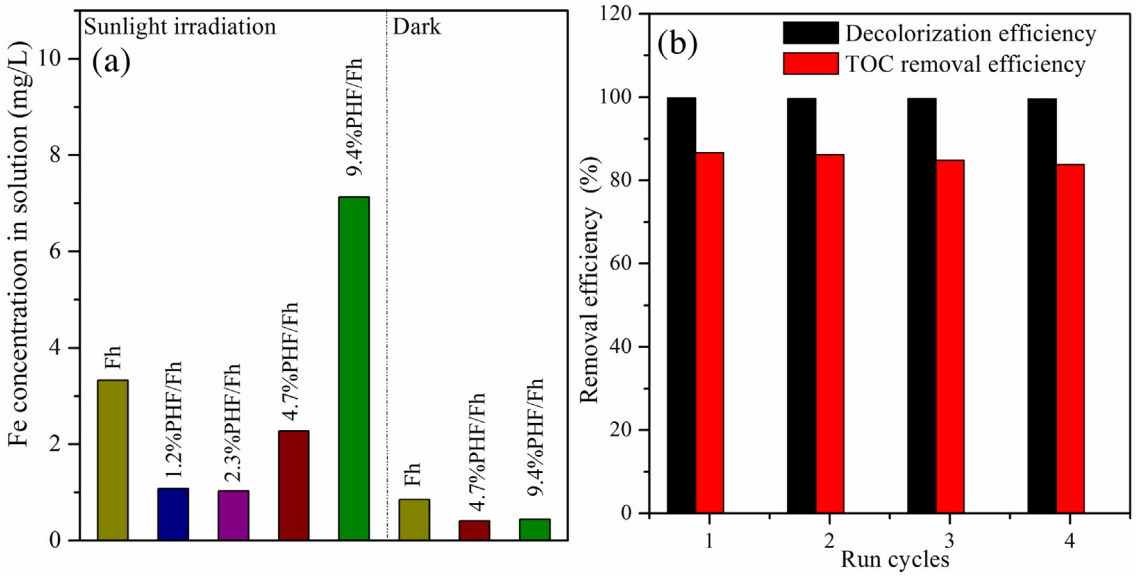

Fig. 5. Fe concentration in solution after 60 min reaction (a) and stability test of 2.3%PHF/Fh (b).

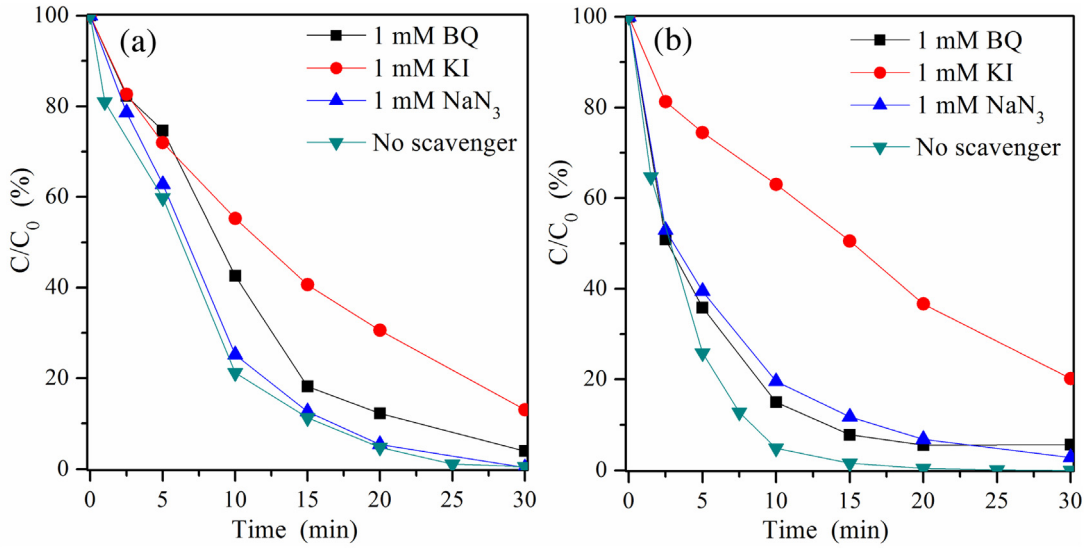

Fig. 6. Decolorization of acid red 18 with the addition of different scavengers. (a) Fh; (b) 2.3%PHF/Fh.

2.4. Photocatalytic tests and analytical methods

The photocatalytic activity of the obtained samples was determined by the degradation of AR18 under various conditions. The experiments were conducted in a photochemical reaction instrument (BL-GHX-V, Shanghai Depai Biotech. Co. Ltd., China). To simulate the sunlight spectrum, a 1000 W xenon lamp (100–105 mW/cm^2) was applied as the light source, which was positioned inside a cylindrical Pyrex vessel surrounded by a circulating water jacket.

In the photocatalytic activity evaluation experiments, 0.4 g/L of sample was added to 50 mL AR18 (2.6×10^{-4} mol/L, pH 3.1) aqueous solution. The initial pH value of the solution was adjusted using 0.1 M NaOH or HNO_3. All experiments were carried out under constant stirring to ensure well dispersion of the samples. The reaction was started when the halogen lamp was turned on and H_2O_2 (0.6×10^{-2} mol/L) was added to AR18 solution. During the photolysis process, the solution was collected at desired intervals, which was followed by centrifugation to separate the solid from the liquid before measurement.

The AR18 concentration was quantified by its absorbance at a wavelength of 509 nm with a spectrophotometer (759S, Shanghai JingHua Instrument Co. Ltd., China). The amount of Fe ions leached from catalysts into the solution was determined by atomic absorption spectrophotometry (PerkinElmer AAnalyst 400, America). Total organic carbon (TOC) was measured by a TOC analyzer (Shimadzu TOC-V CPH, Japan) equipped with an autosampler.

The intermediate products during AR18 degradation were detected by an Agilent7890/5975C GC–MS equipped with a HP-5MS capillary column (60 m × 0.32 mm × 0.25 μm film thickness). The gas chromatographer column was operated in a temperature programmed mode as the following: Initial temperature of 40 °C was held for 10 min, and ramped first to 100 °C with a 12 °C/min rate, then to 200 °C with 5 °C/min, and finally to 280 °C with a 20 °C/min rate, holding for another 5 min.

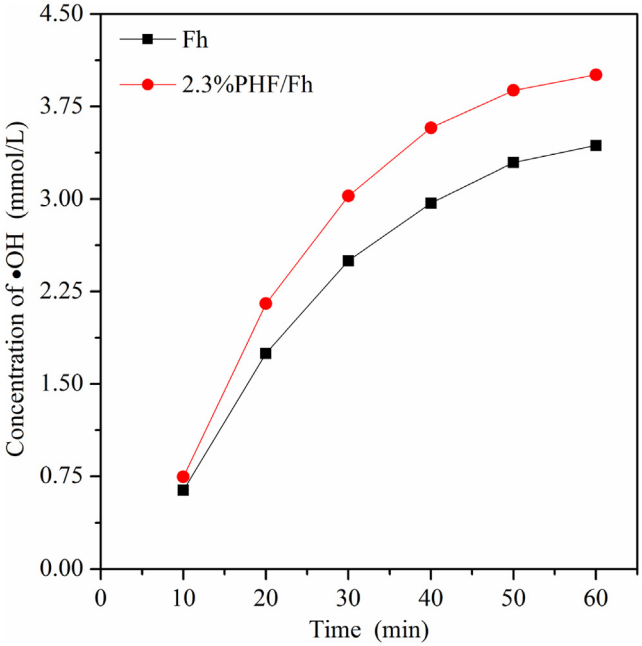

Fig. 7. The concentration of •OH radical in the heterogeneous photo-Fenton systems.

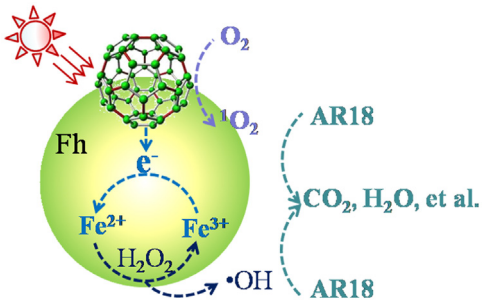

Fig. 8. Possible photocatalytic mechanism.

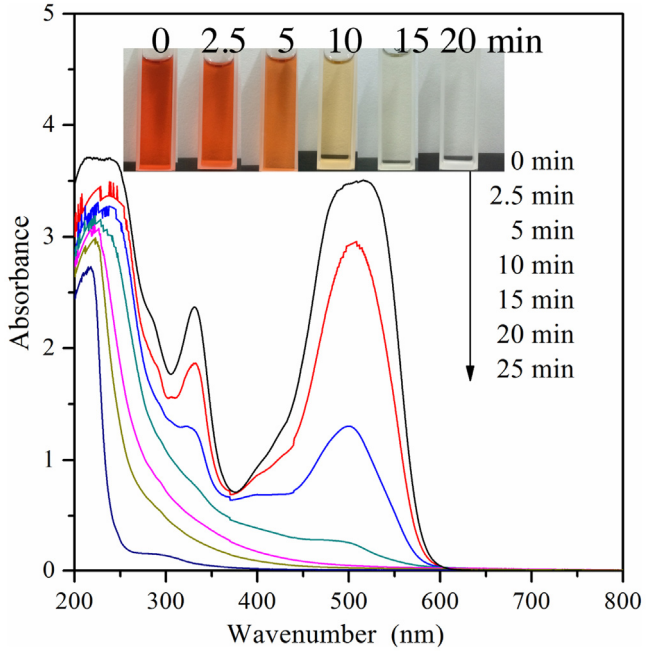

Fig. 9. UV–vis spectral changes of acid red 18 as a function of irradiation time.

2.5. Analysis of reactive species

Free radical capture experiments were used to ascertain the reactive species in the photodegradation process of AR18. Potassium iodide (KI), sodium azide (NaN_3), and benzoquinone (BQ) were chosen as the hydroxyl radical (OH•) scavenger, singlet oxygen ($^1O_2$) scavenger, and superoxide iron radical ($O_2^{\bullet-}$) scavenger [32–34], respectively. The experimental details for free radical capture processes were similar to the photocatalytic experiment.

•OH radicals generated in heterogeneous photo-Fenton processes were trapped with dimethyl sulfoxide (DMSO) to produce formaldehyde quantitatively, and then reacted with 2,4-dinitrophenylhydrazine (DNPH) to form hydrazone ($DNPH_o$), which were analyzed by high performance liquid chromatography (HPLC) [35]. Furfur alcohol (FFA, 10^{-4} mol/L) was used as $^1O_2$ acceptor [36,37], and the residual concentration of FFA was determined by HPLC. The reaction between FFA and $^1O_2$ is diffusion controlled with the expression of Eq. (1),

$$-\mathrm{d[FFA]}/\mathrm{d}t = k_r[^1O_2][\mathrm{FFA}] \quad (1)$$

where $[^1O_2]$ and [FFA] are the concentrations of $^1O_2$ and FFA, respectively. It was reported that k_r for this reaction is $1.2 \times 10^8\ M^{-1}\ s^{-1}$ [36,37]. The values of the pseudo first order rate constant for FFA loss (k_{obs}) was obtained through Eq. (2),

$$-\mathrm{d[FFA]}/\mathrm{d}t = k_{obs}[\mathrm{FFA}] \quad (2)$$

Then, steady-state $^1O_2$ concentrations were calculated by Eq. (3),

$$[^1O_2] = k_{obs}/k_r \quad (3)$$

The details of analysis procedure were described according to the paper of Zhong et al. [35] and Zhang et al. [36].

2.6. Photocatalytic stability experiments

The 2.3%PHF/Fh sample was used repeatedly in the degradation of AR18 to evaluate its photocatalytic stability. The experimental processes were similar to above photocatalytic experiments. After reaction in each run, the sample was collected by centrifugation to separate the solid for the next use.

3. Results and discussion

3.1. Structural characterization results

Two broad peaks were found in the XRD patterns of the samples at 35° and 63° (2θ), respectively (Fig. 1), consistent with previous reports for pure 2-line Fh [38,39], which suggested that the presence of PHF did not significantly affect the structure of Fh. According to the results of element analysis (Table 1), the contents of carbon element for 1.2%PHF/Fh, 2.3%PHF/Fh, 4.7%PHF/Fh, and 9.4%PHF/Fh were 0.81, 1.26, 2.06, and 3.67 wt%, respectively. In addition, the BET data (Table 1) showed that the SSA of all the PHF/Fh samples were less than that of Fh, and decreased with increasing PHF content. Probably, the loaded PHF blocked some of the pores on Fh, leading to a decrease of SSA.

The morphology of the samples was characterized using SEM (Fig. S2), which showed that no evident change for the morphology of Fh before and after the addition of PHF. The particle size and morphology of the samples were further characterized by SPM. As shown in Fig. 2a and b, the particle size of PHF was less than 2 nm,

Table 2
Intermediate products identified by GC–MS.

NO.	Retention time	Compoud identified by GC–MS	Formula	Name	Mw	The major ions (mz)
1	7.058	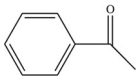	C_8H_8O	Acetophenone	120	43, 51, 77, 105, 120
2	7.250	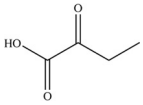	$C_4H_6O_3$	2-Oxobutyric acid1,4-Pentadien-3-ol	102	27, 29, 45, 57
3	13.812	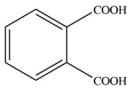	$C_8H_6O_4$	1,2-Benzenedicarboxylic acid	166	50, 74, 76, 104, 148
4	14.370	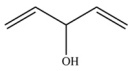	C_5H_8O	1,4-Pentadien-3-ol	84	29, 39, 55, 57, 83
5	21.824	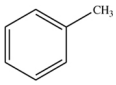	C_7H_8	Toluene	92	39, 63, 65, 91, 92
6	27.626	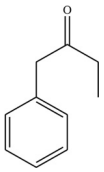	$C_{10}H_{12}O$	1-Phenyl-2-butanone	148	29, 39, 57, 65, 91, 148

and the pure Fh showed approximately spherical particles with the diameter less than 3 nm, in accordance with the results in previous studies [40,41]. PHF/Fh showed larger particle size as compared with PHF and Fh, which may result from the integration of PHF inside Fh since PHF was introduced during the precipitation of Fh. With the increased of PHF content, the heights of the samples with different content of PHF were still less than 12 nm, even after the PHF content reached up to 9.4 wt% (Fig. 2c–f).

The DRS results (Fig. 3) displayed that Fh had good absorption in the whole light region, and the addition of PHF could enhance the absorption intensity. In addition, the absorption intensity increased with increasing PHF content.

3.2. Degradation of AR18

To investigate the effect of PHF on AR18 degradation in the heterogeneous photo-Fenton system, several photocatalytic experiments using the samples with varying PHF contents were carried out for AR18 degradation under various conditions (Fig. 4). Under the dark conditions (Fig. 4a), approximately 25% AR18 was removed by Fh. As Fh shows positively charged surface at pH < 8 and AR18 is an anionic dye, AR18 could be adsorbed to Fh through electrostatic attraction [30,42]. The removal of AR18 by PHF/Fh was reversely related to PHF contents and was lower than that by Fh. PHF was known to have negative charges in the pH range 3.0–9.5 [29], which then might inhibit the adsorption of anionic dyes because of the electrostatic repulsion.

Under simulated sunlight irradiation (Fig. 4b, c), the mineralization of AR18 was negligible without adding H_2O_2 and catalysts, indicating that AR18 can resist decomposition from sunlight. The decolorization rate constant k of pure H_2O_2 on the photocatalytic degradation of AR18 was only 0.085 min^{-1}, and it was further slightly increased after the addition of PHF (*i.e.*, the 'PHF + H_2O_2' system). However, in both the two systems only about 10% TOC of AR18 was removed after 60 min reaction, which indicated that PHF had weak capacity for the decolorization and mineralization of AR18 under the tested conditions.

As for the 'Fh + H_2O_2' system, the decolorization rate and TOC removal of AR18 were obviously faster than those under control conditions. Interestingly, the decolorization rate and TOC removal of AR18 by PHF/Fh composites were higher than those by Fh, although Fh showed better AR18 adsorption capacity (Fig. 4a). In addition, with the increased of PHF content, the degradation rate increased at first due to photo-Fenton reaction, but begun to decrease when the content was above 2.3 wt% because of spatial inhibition. It suggested that both PHF and Fh were important for the photo-Fenton degradation process. Moreover, the degradation rate of AR18 by 2.3%PHF/Fh (0.281 min^{-1}) was nearly twice as that by Fh (0.148 min^{-1}). Furthermore, the TOC removal by 2.3%PHF/Fh (86.7%) after 60 min reaction was significantly higher than that by Fh (69.6%). This phenomenon further implied that the presence of PHF could enhance the photo-Fenton catalytic activity of Fh. The excited state PHF could not only generate $^1O_2$ [4–7], but also could transfer electrons to the Fe^{3+} on Fh [9,31], which can then further promote the decomposition of H_2O_2 into highly oxidative •OH. Hence, the high removal efficiency of AR18 by PHF/Fh might be attributed to the reaction of AR18 with small amounts of $^1O_2$ photosensitized by PHF, or to the increased amounts of •OH produced by the synergetic effect of PHF and Fh.

3.3. Stability test of the samples

In order to determine the stability of the catalysts, Fe concentrations in the solutions after 60 min reaction in different systems were measured (Fig. 5a). Under sunlight irradiation, Fe leaching was approximately 1 mg/L for both 1.2%PHF/Fh and 2.3%PHF/Fh, and 2.2 mg/L for 4.7%PHF/Fh, which were far lower than that for pure Fh (3.4 mg/L). However, Fe leaching was much higher for 9.4%PHF/Fh (7 mg/L). As such, good stability could be obtained for PHF/Fh when the PHF content was lower than 4.7 wt%. Under the dark conditions, it showed that Fe leaching from PHF/Fh was lower than that from pure Fh. Fe leaching contents from 1.2%PHF/Fh and 2.3%PHF/Fh were lower than the limit of AAS detection, which further validated

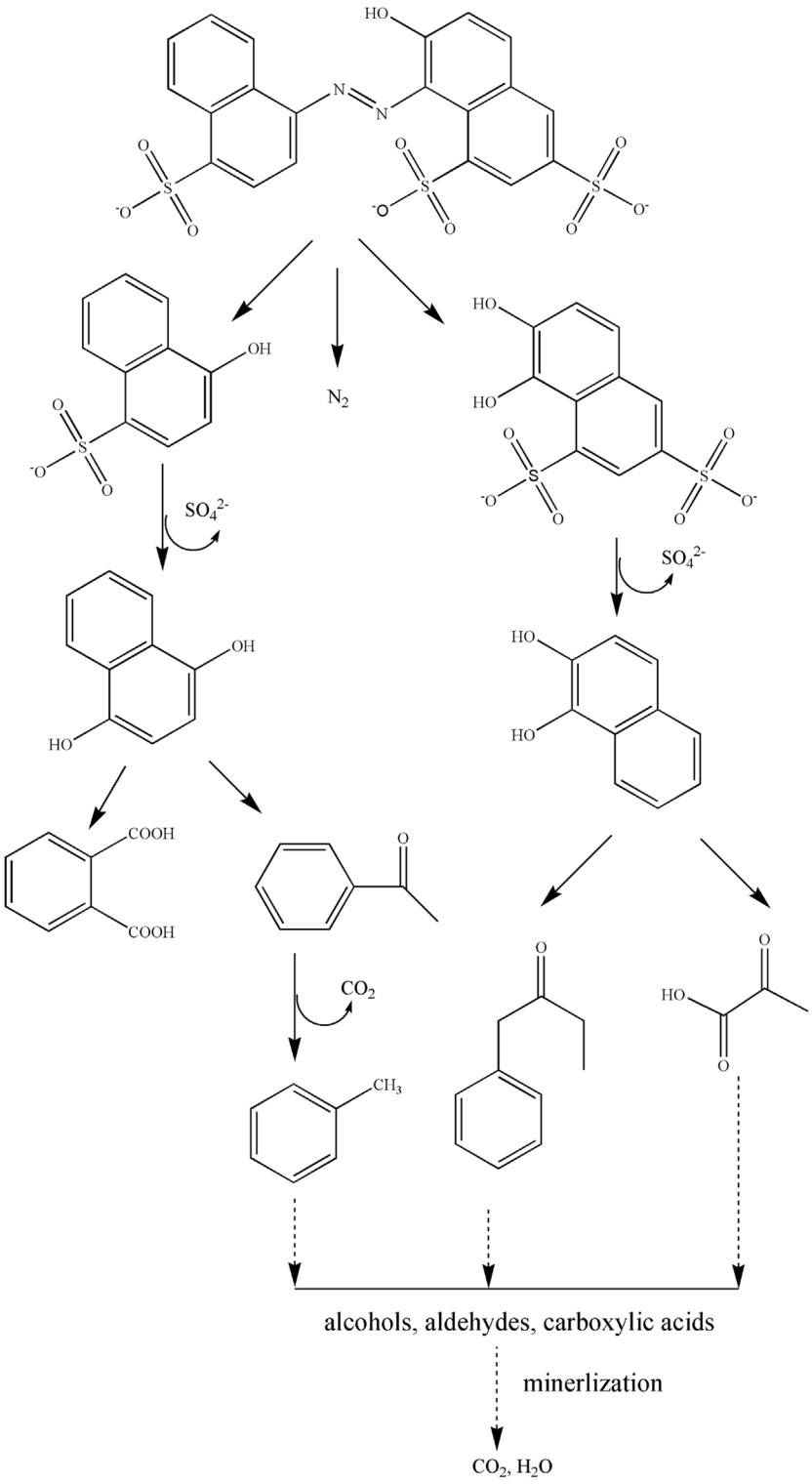

Fig. 10. Possible degradation pathway of acid red 18 in the heterogeneous photo-Fenton process using 2.3%PHF/Fh as catalyst.

that an appropriate amount of PHF could enhance the stability of Fh.

As is well known, the long-term stability of a catalyst is a key issue for its practical application. The results of the stability test of 2.3%PHF/Fh (Fig. 5b) showed that the decolorization efficiency of AR18 (>98%) and TOC removal efficiency (>80%) was still quite efficient after being used for 4 cycles, implying that 2.3%PHF/Fh was very stable.

3.4. Analysis of active oxidative species

Fig. 6 presents the results of active oxidative species analysis in the systems using Fh and 2.3%PHF/Fh as catalysts, which showed different inhibiting effect on AR18 degradation in the two reaction systems. In the Fh system, the decolorization of AR18 was slightly inhibited when NaN_3 ($^1O_2$ scavenger) was added. However, when the $O_2^{\bullet -}$ radical scavenger (BQ) was employed, evident inhibition

was observed in the photocatalytic degradation of AR18, and a more obvious inhibition was observed when •OH radical scavenger (KI) was introduced. Hence, in this system, the main active oxidative specie should be •OH radical, which was followed by $O_2^{\bullet-}$ radical and $^1O_2$. As for the 2.3%PHF/Fh system, the suppression capacity was more obvious as compared with the Fh system when NaN_3 was added. Furthermore, when the •OH radical scavenger (KI) was introduced, the suppression rate in the PHF/Fh system (49%) was higher than that in the Fh system (33%). As such, the main active oxidative specie should be •OH radical as well in the PHF/Fh system, and the contents of both $^1O_2$ and •OH radical in this system were significantly higher than those in the Fh system. Therefore, the presence of PHF could enhance the production of $^1O_2$ and •OH radical in the heterogeneous photo-Fenton process.

To further analyze the effect of PHF on the heterogeneous photo-Fenton process, the concentration of •OH radical and $^1O_2$ in the heterogeneous photo-Fenton systems catalyzed by 2.3%PHF/Fh and Fh were measured. From the trend of •OH radical generation by 2.3%PHF/Fh and Fh (Fig. 7), the yield amount of •OH radical increased sustainably as the reaction continued. In addition, the system catalyzed by 2.3%PHF/Fh clearly generated higher concentration of •OH radical than the system catalyzed by Fh (*e.g.*, 4.0 *vs.* 3.4 mmol/L after 180 min reaction). The remarkable •OH radical generation performance of 2.3%PHF/Fh suggested that the presence of PHF could contribute to accelerating the generation of •OH radical.

The rate constant for FFA loss (k_{obs}) was obtained from the slope of a straight line by plotting the value of $\ln([FFA]_0/[FFA])$ against the reaction time (Fig. S3). It clearly showed that the k_{obs} by 2.3%PHF/Fh (1×10^{-4} s^{-1}) was higher than that by Fh (4×10^{-5} s^{-1}). Furthermore, the corresponding steady-state $^1O_2$ concentrations produced by Fh and 2.3%PHF/Fh was 8.3×10^{-13} and 3.3×10^{-13} M, respectively, implying that introducing PHF to Fh could greatly enhance the production of $^1O_2$ in the heterogeneous photo-Fenton process. Based on above results, the possible contributions for the enhanced photocatalytic activity of 2.3%PHF/Fh might originate from two aspects (Fig. 8). The first one might originate from the excited state PHF, which can efficiently sensitize the ground state triplet oxygen to generate $^1O_2$ [4–7]. Another one might be attributed to the synergetic effect between PHF and Fh, and the excited state PHF could reduce and transfer electrons to the Fe^{3+} on Fh due to $E^0(C_{60}^+/^1C_{60}^*) = 0.1$ V *vs.* NHE < $E^0(Fe^{3+}/Fe^{2+}) = 0.77$ V *vs.* NHE [9,31]. Subsequently, the reduction of Fe^{3+} into Fe^{2+} can be accelerated, which then can further promote the decomposition of H_2O_2 into highly oxidative •OH radical.

3.5. Possible degradation pathway for the degradation of AR18

Generally, the color of dye is formed by the cooperation of chromophore and auxochrome [43–45]. As such, decolorization of AR18 can be achieved once the azo bond (—N=N—) is broken [46]. The UV–vis spectra recorded during photodegradation of AR18 are presented in Fig. 9. The spectrum of AR18 before photodegradation (t = 0 min) exhibited two main peaks at the wavelengths of 509 and 332 nm, respectively, and the absorption at 509 nm is related to the N=N group of AR18 [47]. The results showed that the intensity of the absorption peaks at 509 nm decreased rapidly after photolysis, without the appearance of new absorption peaks.

The bond lengths and bond angles of AR18 were calculated by density functional theory (DFT) method at the B3LYP/6-311G level with the GAMESS (Table S1). In organic chemical reactions, the benzene ring is generally more stable than the line structure; the azo bond is especially easy to be attacked by free radicals in advanced oxidation process [48]. The bond angles and lengths were compared (Table S1), the lengths of C(7)—N(11), N(11)—N(12), and N(12)—C(13) were 1.444, 1.377, and 1.445 Å, respectively, implying that the N(12)—C(13) bond should be the firstly broken. The intermediate products of AR18 degradation were examined using GC–MS (Table 2). Based on the results of the GAMESS calculation and GC–MS analysis, the possible degradation pathway was proposed (Fig. 10). First, the C—N bond (—C—N=N—) would be broken, and then nitrogen atoms could be released as the form of nitrogen or ammonia. Further oxidation then gave rise to substituted benzene compounds as intermediates, such as acetophenone, 1,2-benzenedicarboxylic acid, toluene, and 1-phenyl-2-butanone. With the continuous oxidation, the aromatic rings were opened, which were responsible for the formation of alcohols, aldehydes, and carboxylic acids (e.g., 2-oxobutyric acid and 1,4-pentadien-3-ol). Finally, these intermediate products were converted to carbon dioxide and water.

4. Conclusion

PHF can significantly affect the heterogeneous photo-Fenton activity of Fh in the degradation of AR18. The obtained PHF/Fh composites exhibited much higher catalytic activities and better structural stability than pure Fh in degrading AR18 under sunlight irradiation. The degradation rate of AR18 by 2.3%PHF/Fh was nearly twice as that by Fh, and TOC removal after 60 min reaction by 2.3%PHF/Fh (86.7%) was much higher than that by Fh (69.6%). The results showed that the presence of PHF could enhance the production of $^1O_2$ and •OH radical. On one hand, the excited state PHF could efficiently sensitize the ground state triplet oxygen to generate $^1O_2$; on the other hand, the electrons transferred from the excited state PHF to Fe^{3+} on Fh could accelerate reduction of Fe^{3+} into Fe^{2+}. Based on the obtained results, a possible reaction pathway for the degradation of AR18 over the PHF/Fh was proposed. AR18 degradation was initiated by the cleavage of C—N bond, which was followed by the production of substituted benzene compounds as intermediates. These intermediates were finally oxidized to carbon dioxide and water by free radicals.

Acknowledgements

This work was financially supported by National Natural Science Foundation of China (41572031, 41322014), National Youth Top-notch Talent Support Program, Newton Advanced Fellowship (NA150190), CAS/SAFEA International Partnership Program for Creative Research Teams (20140491534), and Guangdong Provincial Youth Top-notch Talent Support Program (2014TQ01Z249). This is a contribution (No. IS-2297) from GIGCAS.

Appendix A. Supplementary data

Supplementary data associated with this article can be found, in the online version, at http://dx.doi.org/10.1016/j.molcata.2016.09.024.

References

[1] L. Ge, K. Moor, B. Zhang, Y. He, J.H. Kim, Electron transfer mediation by aqueous C_{60} aggregates in H_2O_2/UV advanced oxidation of indigo carmine, Nanoscale 6 (22) (2014) 13579–13585.
[2] K. Pichler, S. Graham, O.M. Gelsen, R.H. Friend, W.J. Romanow, J.P. Mccauley, N. Coustel, J.E. Fischer, A.B. Smith, Photophysical properties of solid films of fullerene, C_{60}, Microporous Mesoporous Mater. 203 (47) (2015) 163–169.
[3] M.F. Lo, Z.Q. Guan, T.W. Ng, C.Y. Chan, C.S. Lee, Electronic structures and photoconversion mechanism in Perovskite/Fullerene heterojunctions, Adv. Funct. Mater. 25 (8) (2015) 1213–1218.
[4] P. Mroz, G.P. Tegos, H. Gali, T. Wharton, T. Sarna, M.R. Hamblin, Photodynamic therapy with fullerenes, Photochem. Photobiol. Sci. 6 (11) (2007) 1139–1149.
[5] K.D. Pickering, M.R. Wiesner, Fullerol-sensitized production of reactive oxygen species in aqueous solution, Environ. Sci. Technol. 39 (5) (2005) 1359–1365.

[6] K.J. Moor, J.H. Kim, Simple synthetic method toward solid supported C_{60} visible light-activated photocatalysts, Environ. Sci. Technol. 48 (5) (2014) 2785–2791.
[7] J. Lee, S. Hong, Y. Mackeyev, C. Lee, E. Chung, L.J. Wilson, J.H. Kim, P.J.J. Alvarez, Photosensitized oxidation of emerging organic pollutants by tetrakis C_{60} aminofullerene-derivatized silica under visible light irradiation, Environ. Sci. Technol. 45 (24) (2011) 10598–10604.
[8] D.M. Guldi, M. Prato, Excited-state properties of C(60) fullerene derivatives, Acc. Chem. Res. 33 (10) (2000) 695–703.
[9] Y. Park, N.J. Singh, K.S. Kim, T. Tachikawa, T. Majima, W. Choi, Fullerol–titania charge-transfer-mediated photocatalysis working under visible light, Chemistry 15 (41) (2009) 10843–10850.
[10] W. Bai, V. Krishna, J. Wang, B. Moudgil, B. Koopman, Enhancement of nano titanium dioxide photocatalysis in transparent coatings by polyhydroxy fullerene, Appl. Catal. B Environ. 125 (3) (2012) 128–135.
[11] Z.D. Meng, M.M. Peng, L. Zhu, W.C. Oh, F.J. Zhang, Fullerene modification CdS/TiO_2 to enhancement surface area and modification of photocatalytic activity under visible light, Appl. Catal. B Environ. 113–114 (2012) 141–149.
[12] H. Fu, T. Xu, S. Zhu, Y. Zhu, Photocorrosion inhibition and enhancement of photocatalytic activity for ZnO via hybridization with C_{60}, Environ. Sci. Technol. 42 (21) (2008) 8064–8069.
[13] Shengbao Zhu, Tongguang Xu, Hongbo Fu, A. Jincai Zhao, Yongfa Zhu, Synergetic effect of Bi_2WO_6 photocatalyst with C_{60} and enhanced photoactivity under visible irradiation, Environ. Sci. Technol. 41 (17) (2007) 6234–6239.
[14] J. Herney-Ramirez, M.A. Vicente, L.M. Madeira, Heterogeneous photo-Fenton oxidation with pillared clay-based catalysts for wastewater treatment: a review, Appl. Catal. B Environ. 98 (1–2) (2010) 10–26.
[15] X. Li, Prussian blue/TiO_2 nanocomposites as a heterogeneous photo-Fenton catalyst for degradation of organic pollutants in water, Catal. Sci. Technol. 5 (1) (2014) 504–514.
[16] N.S. Ai, B.H. Hameed, Heterogeneous catalytic treatment of synthetic dyes in aqueous media using Fenton and photo-assisted Fenton process, Desalination 269 (1–3) (2011) 1–16.
[17] O.S.N. Sum, J. Feng, X. Hub, P.L. Yue, Photo-assisted fenton mineralization of an azo-dye acid black 1 using a modified laponite clay-based Fe nanocomposite as a heterogeneous catalyst, Top. Catal. 33 (1) (2005) 233–242.
[18] T. Xu, R. Zhu, J. Zhu, X. Liang, Y. Liu, Y. Xu, H. He, $BiVO_4$/Fe/Mt composite for visible-light-driven degradation of acid red 18, Appl. Clay Sci. 129 (2016) 27–34.
[19] X. Yang, W. Chen, J. Huang, Y. Zhou, Y. Zhu, C. Li, Rapid degradation of methylene blue in a novel heterogeneous Fe_3O_4@rGO@TiO_2-catalyzed photo-Fenton system, Sci. Rep. 5 (2015) 10632.
[20] P. Avetta, A. Pensato, M. Minella, M. Malandrino, V. Maurino, C. Minero, K. Hanna, D. Vione, Activation of persulfate by irradiated magnetite: implications for the degradation of phenol under heterogeneous photo-Fenton-like conditions, Environ. Sci. Technol. 49 (2) (2015) 15883–15891.
[21] Y. Zhang, G.U. Yan, H. Yang, H.E. Yan, L.I. Rui-Ping, Y.P. Huang, A.Q. Zhang, Degradation of organic pollutants by photo-Fenton-like system with hematite, Environ. Sci. 33 (4) (2012) 1247–1251.
[22] G.B.O.D.L. Plata, O.M. Alfano, A.E. Cassano, Decomposition of 2-chlorophenol employing goethite as Fenton catalyst II: reaction kinetics of the heterogeneous Fenton and photo-Fenton mechanisms, Appl. Catal. B Environ. 95 (1) (2010) 14–25.
[23] J. Cervini-Silva, A.N. Camacho, E. Palacios, P.D. Angel, M. Pentrak, L. Pentrakova, S. Kaufhold, K. Ufer, M.T. Ramírez-Apan, V. Gómez-Vidales, Anti-inflammatory, antibacterial, and cytotoxic activity by natural matrices of nano-iron(hydr)oxide/halloysite, Appl. Clay Sci. 120 (2015) 101–110.
[24] X. Zhang, Y. Chen, N. Zhao, H. Liu, Y. Wei, Citrate modified ferrihydrite microstructures: facile synthesis, strong adsorption and excellent Fenton-like catalytic properties, RSC Adv. 4 (41) (2014) 21575–21583.
[25] J.C. Barreiro, M.D. Capelato, L. Martin-Neto, H.C.B. Hansen, Oxidative decomposition of atrazine by a Fenton-like reaction in a H_2O_2/ferrihydrite system, Water Res. 41 (1) (2007) 55–62.
[26] P.V. Hong, J.W. Moreau, Thiocyanate adsorption on ferrihydrite and its fate during ferrihydrite transformation to hematite and goethite, Chemosphere 119 (119C) (2015) 987–993.
[27] P. Qi, T. Pichler, Closer look at As(III) and As(V) adsorption onto ferrihydrite under competitive conditions, Langmuir 30 (37) (2014) 11110–11116.
[28] Y. Wang, Y. Zhao, Y. Ma, H. Liu, Y. Wei, Photo-oxidation of Mordant Yellow 10 in aqueous dispersions of ferrihydrite and H_2O_2, J. Mol. Catal. A Chem. 325 (2010) 79–83.
[29] P.A. Indeglia, A. Georgieva, V.B. Krishna, J.C.J. Bonzongo, Physicochemical characterization of fullerenol and fullerenol synthesis by-products prepared in alkaline media, J. Nanopart. Res. 16 (2599) (2014) 1–15.
[30] J. Antelo, S. Fiol, C. Pérez, S. Mariño, F. Arce, D. Gondar, R. López, Analysis of phosphate adsorption onto ferrihydrite using the CD-MUSIC model, J. Colloid Interface Sci. 347 (1) (2010) 112–119.
[31] Z. Wang, D. Luan, S. Madhavi, C.M. Li, X.W. Lou, α-Fe_2O_3 nanotubes with superior lithium storage capability, Chem. Commun. 47 (28) (2011) 8061–8063.
[32] W. Li, S. Zhao, B. Qi, Y. Du, X. Wang, M. Huo, Fast catalytic degradation of organic dye with air and MoO_3:Ce nanofibers under room condition, Appl. Catal. B Environ. 92 (3–4) (2009) 333–340.
[33] C. Lalhriatpuia, D. Tiwari, A. Tiwari, S.M. Lee, Immobilized nanopillars-TiO_2 in the efficient removal of micro-pollutants from aqueous solutions: physico-chemical studies, Chem. Eng. J. 281 (2015) 782–792.
[34] D. Asai, A. Okada, S. Kondo, K. Tsuda, Photosensitized polymerizations of styrene and methyl methacrylate by tetraphenylphosphonium salts, J. Macromol. Sci. Part A Chem. 6 (1982) 1011–1020.
[35] Y. Zhong, X. Liang, Z. He, W. Tan, J. Zhu, P. Yuan, R. Zhu, H. He, The constraints of transition metal substitutions (Ti, Cr, Mn, Co and Ni) in magnetite on its catalytic activity in heterogeneous Fenton and UV/Fenton reaction: from the perspective of hydroxyl radical generation, Appl. Catal. B Environ. 150 (2014) 612–618.
[36] T. Zhang, Y. Ding, H. Tang, Generation of singlet oxygen over Bi(V)/Bi(III) composite and its use for oxidative degradation of organic pollutants, Chem. Eng. J. 264 (2015) 681–689.
[37] W.R. Haag, J.R. Hoigneí, E. Gassman, A.M. Braun, Singlet oxygen in surface waters—part I: furfuryl alcohol as a trapping agent, Chemosphere 13 (5) (1984) 631–640.
[38] R.K. Kukkadapu, Transformation of 2-line ferrihydrite to 6-line ferrihydrite under oxic and anoxic conditions, Am. Mineral. 88 (11) (2003) 1903–1914.
[39] S. Das, M.J. Hendry, J. Essilfiedughan, Effects of adsorbed arsenate on the rate of transformation of 2-line ferrihydrite at pH 10, Environ. Sci. Technol. 45 (13) (2011) 5557–5563.
[40] K. Kokubo, S. Shirakawa, N. Kobayashi, H. Aoshima, T. Oshima, Facile and scalable synthesis of a highly hydroxylated water-soluble fullerenol as a single nanoparticle, Nano Res. 4 (2) (2011) 204–215.
[41] J.L. Jambor, J.E. Dutrizac, ChemInform abstract: occurrence and constitution of natural and synthetic ferrihydrite, a widespread iron oxyhydroxide, Cheminform 98 (7) (1998) 2549–2586.
[42] S. Wang, Y.Y. Zhai, Q. Gao, W.J. Luo, H. Xia, C.G. Zhou, Highly efficient removal of acid red 18 from aqueous solution by magnetically retrievable chitosan/carbon nanotube: batch study, isotherms, kinetics, and thermodynamics, J. Chem. Eng. Data 59 (1) (2013) 39–51.
[43] Y. Xu, X. Li, X. Cheng, D. Sun, X. Wang, Degradation of cationic red GTL by catalytic wet air oxidation over Mo-Zn-Al-O catalyst under room temperature and atmospheric pressure, Environ. Sci. Technol. 46 (5) (2012) 2856–2863.
[44] A.D. Bokare, R.C. Chikate, C.V. Rode, K.M. Paknikar, Effect of surface chemistry of Fe-Ni nanoparticles on mechanistic pathways of azo dye degradation, Environ. Sci. Technol. 41 (21) (2007) 7437–7443.
[45] C. Chen, Q. Wang, P. Lei, W. Song, W. Ma, J. Zhao, Photodegradation of dye pollutants catalyzed by porous $K_3PW_{12}O_{40}$ under visible irradiation, Environ. Sci. Technol. 40 (12) (2006) 3965–3970.
[46] M.P. Shah, Eco-friendly treatment of acid red by an application of pseudomonas spp, Int. J. Environ. Biorem. Biodegrad. 2 (2) (2014) 62–68.
[47] S. Mozia, M. Tomaszewska, A.W. Morawski, Photocatalytic degradation of azo-dye acid red 18, Desalination 185 (1–3) (2005) 449–456.
[48] L.L. And, Q. Dai, High performance on the degradation of cationic red X-GRL by wet electrocatalytic oxidation process, Ind. Eng. Chem. Res. 46 (26) (2007) 8951–8958.